Measurement and Modeling of the TDR Signal Propagation through Layered Dielectric Media

M. G. Schaap,* D. A. Robinson, S. P. Friedman, and A. Lazar

ABSTRACT

Layered dielectric materials are often encountered in the natural environment due to differences in water content caused either by a wetting or drying front. This is especially true for coarse-grained materials such as sandy soils, sediments, and some rocks that have very distinctive layers of water content. This paper examines the issue of how the permittivity along a time domain reflectometry (TDR) probe is averaged as a function of layer thickness and probe orientation. Measurements of apparent permittivity using TDR are presented for two-, three-, and multi-layer materials. Time domain reflectometry waveforms are modeled for multiple layers of varying thickness and show a change in the averaging of the apparent permittivity from refractive index to arithmetic when more thin layers are present. Analysis of the modeled results shows that the averaging regime is frequency-dependent. However, broadband techniques applied to materials with a few layers will generally produce refractive averaging. A transition to arithmetic averaging is found for systems having many (>4 layers). Narrow-band methods may be very sensitive to layering and may perform in a highly non-refractive way when layering with a strong permittivity contrast is present.

Layering of soils and sediments due to sedimentary or pedogenic processes is common in the natural environment. The individual layers of such systems often have distinct physical properties, such as different textural distributions, densities, and compositions, which in turn may give rise to differences in water content among the layers. An extreme example of a multi-layer material might be modern or ancient lakebed sediments where seasonal variations in deposition cause banding of the material such as varve deposits found in Sweden and elsewhere (Björck et al., 1992). Layered water contents may also occur in homogeneous coarse material, just above the phreatic surface or after infiltration events. In many circumstances it is of interest to determine the average water content of a layered soil or sediment using dielectric methods such as TDR or ground-penetrating radar (GPR). Topp et al. (1982) used TDR to determine the average water content over depth while Todoroff and Lan Sun Luk (2001) inversely determined the depth of the wetting front. Similar techniques were used to determine the unfrozen water content or depth of permafrost (Stein and Kane, 1983; Hayhoe et al., 1983). With GPR it is possible to provide two-dimensional vertical transects within fields to determine wetting front locations and density changes (Huisman et al., 2001). All of these applications require understanding of how electromagnetic waves propagate through layered media.

Early studies that applied TDR to determine the effective permittivity of layered materials showed encouraging results. For example, Birchack et al. (1974) presented a model based on layers, as did Topp et al. (1982), and the method was later named the refractive index mixing method (Whalley, 1993). Topp's derivation is a simple model for two layers based on the summation of propagation times, describing the apparent, measured permittivity (K_a) as:

$$K_a = \left(\frac{L_1\sqrt{K_1} + L_2\sqrt{K_2}}{L}\right)^2 \qquad [1]$$

Where, L is the total length of the measurement, L_1 is the length of the first layer with permittivity K_1 and L_2 is the length of the second layer with permittivity of K_2. This has been further investigated by Nadler et al. (1991) who found reasonable correspondence with Topps model (Topp et al., 1980). However, both Nadler et al. (1991) and Dasberg and Hopmans (1992) pointed out the difficulty that arose with interpreting their waveforms from TDR data in layered media.

Recently Chan and Knight (1999; 2001) demonstrated that the concept of simply summing propagation times in layers is not always correct and that the averaging of propagation velocity changes with the ratio of effective wavelength (λ) to layer thickness (t) (Fig. 1). They suggested (Chan and Knight, 2001) that a transition zone exists where the ratio is about 4; this corresponds to a layer thickness of a quarter wavelength. Chan and Knight (2001) used an equation for which they adopted the term ray theory for the situation where the ratio is smaller than 4:

$$v_{\text{ray}} = \frac{1}{\frac{1}{f_1 v_1} + \frac{1}{f_2 v_2}} \qquad \lambda/t < 4 \qquad [2]$$

Where f_1 is the length fraction for a material with wave propagation velocity of v_1. Ray theory is equivalent to refractive index mixing of permittivity $\sqrt{K_a} = \sqrt{K_1}f_1 + \sqrt{K_2}f_2$ (Eq. [1]) where K_1 is the permittivity of that section.

Above values of 4 what they termed effective medium theory (EMT) is valid:

$$v_{\text{EMT}} = \left(\frac{1}{\sqrt{\frac{f_1}{\sqrt{v_1}} + \frac{f_2}{\sqrt{v_2}}}}\right)^2 \qquad \lambda/t > 4 \qquad [3]$$

M.G. Schaap and D.A. Robinson, George E. Brown Jr., Salinity Lab., 450 W. Big Springs Rd., Riverside, CA 92507. S.P. Friedman and A. Lazar, The Institute of Soil, Water and Environmental Sciences, (ARO) The Volcani Center, Bet Dagan, Israel. Received 26 July 2002. *Corresponding author (mschaap@ussl.ars.usda.gov).

Published in Soil Sci. Soc. Am. J. 67:1113–1121 (2003).

Abbreviations: EC, electrical conductivity; EMT, effective medium theory; GPR, ground-penetrating radar; TDR, time domain reflectometry.

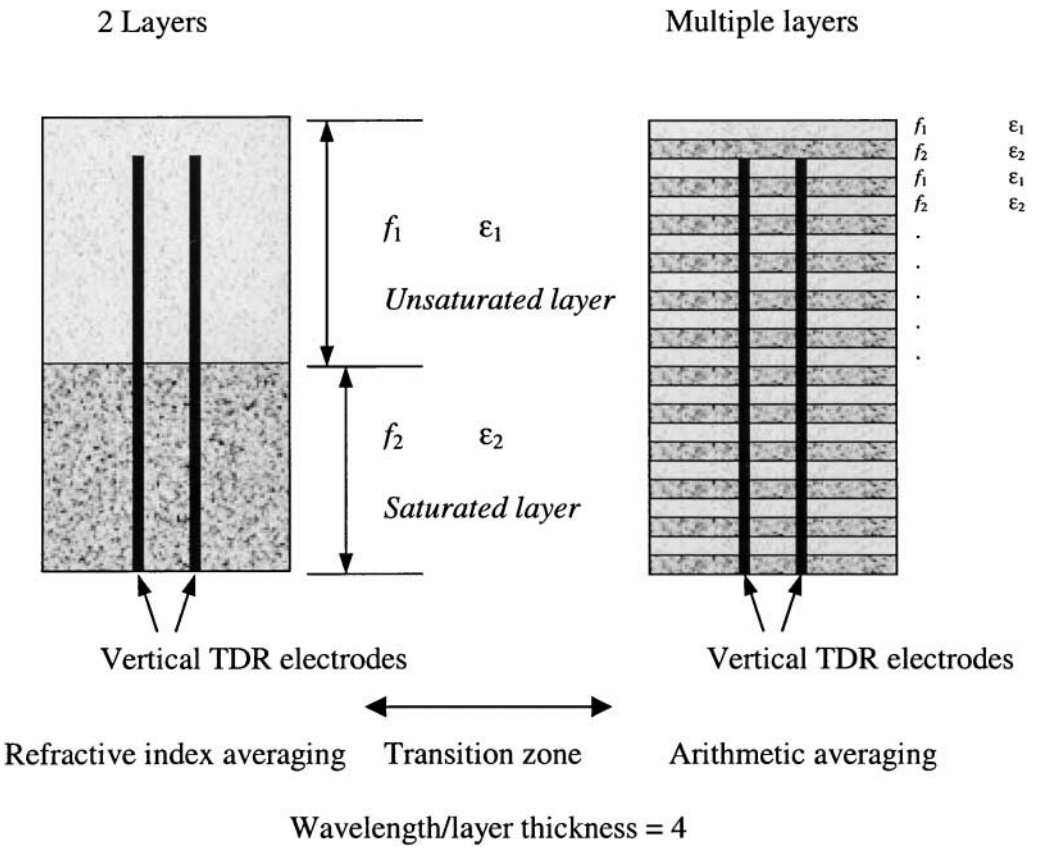

Fig. 1. Schematic diagram showing two-layer and multiple-layer dielectric configurations with reference to the TDR electrodes.

Which is equivalent to the arithmetic averaging of permittivity $K_a = K_1 f_1 + K_2 f_2$.

The choice between refractive and arithmetic averaging has important consequences for the interpretation of water content from TDR or related measurements of apparent permittivity in layered media. In this study we investigate which averaging regime should be used for layered materials, and under what circumstances. To this end we performed measurements on two-, three-, and multi-layered systems. We will also present computed results based on electromagnetic wave propagation theory for the multi-layer system and compare these with the measurements and discuss the causes of a transition between refractive and arithmetic averaging.

MATERIALS AND METHODS

TDR Measurements

Permittivity measurements were made using a Tektronix (1502C) TDR cable tester (Tektronix, Beaverton, OR). The cable tester was connected to a personal computer, which was used to collect and analyze waveforms using software developed by Heimovaara and de Water (1993). The cable tester was connected to different TDR probes for the different experiments. The probes were calibrated for effective length using deionized water and air in a similar manner to Robinson et al. (2003). All experiments were conducted at a constant temperature of 25 ± 0.5°C.

Characterization of Averaging in Air and Water

Experiments were conducted with three-rod TDR probes with a water–air interface forming two layers. Both the permittivity and the electrical conductivity (EC) were measured with the cable tester. In the first experiment the probe was initially held parallel to the water–air interface and was then rotated about the interface until it was vertically immersed in the water (Fig. 2). In a second experiment, the 20-cm probe was inserted perpendicular to the air–water interface 1 cm at a time until the probe was fully immersed in the water (Fig. 2).

Three-Layer Experiments

The three-layer experiment was performed using a seven-wire probe similar to the one described by Heimovaara (1993). The probe was 15 cm long with a spacing of 1.5 cm between the inner and outer 3-mm thick conductors. A plastic outer sheath into which the fluids were poured to give the three phases surrounded the cell. White paraffin (with a relative permittivity of 2.3), water (78.5), and air (1) were the three materials filling the measuring cell from the base upwards.

Multi-Layer Experiment

This experiment was conducted using a two-rod probe with 2-mm thick electrodes, 30.24 cm long at 1.2 cm center spacing. Holes were drilled in 5-cm diameter acrylic disks corresponding with the probe electrodes; the disks were 0.378 cm thick and 80 disks filled the length of the probe. Figure 3 shows a photograph of the probe with 40 disks placed on it, separated by an equal distance in which de-aired water was placed and held using an outer sheath. The disks could be manipulated to give layers of Acrylic and water of differing thickness. Layers corresponded to thicknesses of 0.38, 0.76, 1.52, 1.90, 3.04, 3.80, 7.60, and 15.20 cm. The waveforms retrieved from a multiple-layer medium are noisy and difficult to interpret. To ensure correct interpretation the waveguide was shorted

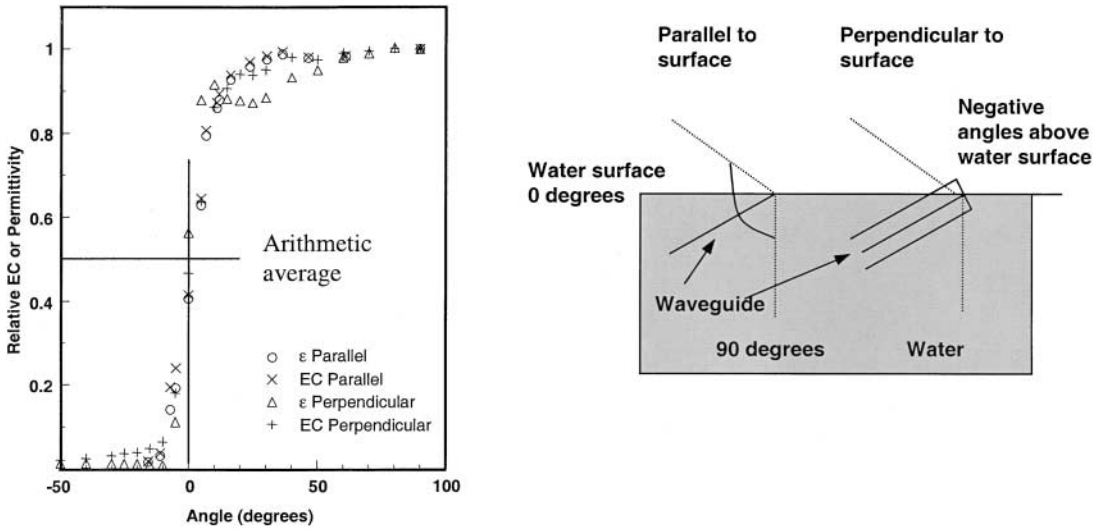

Fig. 2. The relative permittivity (ε) or electrical conductivity (EC) measured using a TDR probe. Zero degrees represents the probe on the water surface, half in, half out. A negative angle indicates the probe in air and a positive angle the probe in water.

across the end after the waveforms were collected so the end point could be determined with some certainty. The waveforms were printed off and the waveform analysis was done by visually fitting the tangents.

TDR Signal Modeling Theory

Time domain reflectometry waveforms result from signals that are reflected at impedance discontinuities between a cable tester and the end of a cable-transmission line system. The cable tester emits a broad spectrum of input frequencies into the cable, and the signal received back often consists of a complex pattern of multiple reflected signals and dielectric losses within the cable-transmission line system. Analysis and modeling of TDR waveforms is most easily and efficiently done in the frequency domain by convolution of an input signal, V_o, with the S_{11} scatter function that contains all the relevant electromagnetic properties of the cable-probe system. The response function R at frequency f is calculated as

$$R(f) = V_o(f)S_{11}(f) \quad [4]$$

$R(f)$, $V_o(f)$, and $S_{11}(f)$ are all complex quantities that can either be given as real and imaginary parts, or as magnitude and phase.

Composite Scatter Function for a Segmented Probe

Heimovaara (1994) used a special probe design that required only the scatter function of the sensor to be known. In this study we consider a probe that consists of multiple segments, each with a separate scatter function. Feng et al. (1999) showed how to compute effective scatter functions for such segmented systems. In essence their theory involves determining the impedances, propagation constants, and reflection coefficients for individual segments, after which the effective scatter function can be computed with

$$S_{11}^k(f) = \frac{\rho_s^k(f) + S_{11}^{k+1}(f)H^k(f, 2L_s^k)}{1 + \rho_s^k(f)S_{11}^{k+1}(f)H^k(f, 2L_s^k)} \quad [5]$$

where k is the segment number, ranging from 1 (the first segment in the probe) to the number of segments N. Equation [5] is recursive, meaning that to compute the scatter function for the entire system (i.e., $k = 1$) is necessary to subsequently compute the $S_{11}^k(f)$ for $k = N, N-1, \ldots 3, 2$, and finally 1. The scatter function for $k = N$ is computed by setting $S_{11}^{N+1}(f)$ equal to the end reflection, which is 1 and -1 for open-ended and shorted probes, respectively (see also Feng et al., 1999). The reflection coefficient $\rho_s^k(f)$ is computed according to

$$\rho_s^k = \frac{Z_{k-1}(f) - Z_k(f)}{Z_{k-1}(f) + Z_k(f)} \quad [6]$$

where $Z_k(f)$ is the impedance for segment k at frequency f; Z_0 is equal to the impedance of the cable that is attached to the probe, in our case 50 ohms. The propagation function $H^k(f,x)$ is computed according to

$$H(f, x) = \exp(-\gamma x) \quad [7]$$

where x is a placeholder for the segment length (L_s in Eq. [5]) and γ is the propagation constant, which is computed as

$$\gamma = \sqrt{(i2\pi fL + R_s)(i2\pi fC + G)} \quad [8]$$

where i denotes a complex quantity and L and C are the inductance and capacitance of the segment, respectively. R_s and G are the skin-resistance of the conductor and the conduc-

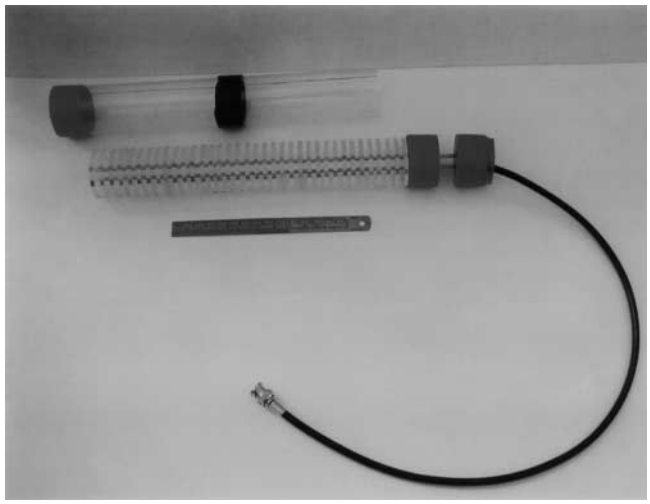

Fig. 3. Photograph of the multi-layer probe with 5-cm diam. Acrylic disks spaced 0.38 cm apart.

tance of the medium, respectively. For the purposes of this study, both will be set to zero.

The quantities Z, L, and C are dependent on the magnetic (L) and dielectric properties (C) of the medium and also depend on the geometry of the probe. For two-rod probes the following expressions hold (Davidson, 1978):

$$L = \frac{\mu}{\pi}\cosh^{-1}(D/d) \quad [9]$$

$$C = \frac{\pi\varepsilon^*}{\cosh^{-1}(D/d)} \quad [10]$$

$$Z = \sqrt{L/C} = \frac{1}{\pi}\sqrt{\mu/\varepsilon^*}\ \cosh^{-1}(D/d) \quad [11]$$

where D is the center to center spacing of two rods, and d is the rod diameter. The medium we studied had no magnetic properties and we therefore set the magnetic permeability, μ, to that of vacuum (μ_0). Because of the relaxation of water the complex dielectric permittivity, ε^*, is frequency-dependent and was computed with the Debeye equation

$$\varepsilon^* = \varepsilon_\infty + \frac{\varepsilon_s - \varepsilon_\infty}{1 + if/f_{rel}} \quad [12]$$

where ε_s and ε_∞ are the static permittivity and permittivity at infinite frequency, respectively, f_{rel} is the relaxation frequency of water. For the Acrylic ε^* was assumed constant for all frequencies.

Calculation of TDR Waveforms

To compute modeled waveforms an input function V_o (Eq. [4]) is necessary. Heimovaara (1994) determined V_o by measuring the open-ended reflection of the probe head. However, determining an input signal in this way is somewhat problematic because even at the output port of a Tektronix 1502B cable tester the signal already has undergone some internal reflections that contaminate the signal. In addition cable connectors may also cause some small reflections. A relatively clean input signal can be determined by using a procedure outlined by Huisman et al. (2002). In this approach, open and short-circuited time-domain waveforms [$W_o(t)$ and $W_s(t)$] were measured by connecting standard open and short calibration loads (Model 8550Q, Maury Microwave Corp., Ontario, CA) to the port of the cable tester. A waveform with minimal internal reflections is then computed by

$$W(t) = [W_o(t) - W_s(t)]/2. \quad [13]$$

The $W_o(t)$ and $W_s(t)$ signals were acquired with a program developed by Heimovaara (1994) that was modified to measure 16 384 points from −0.5 m to approximately 65 m. The input signal $V_o(f)$ was computed by taking the back difference of $W(t)$, followed by a Fast Fourier Transform (Heimovaara, 1994). The input signal frequencies range from 0 to 37.1150 GHz, in steps of 4.5312 MHz. Inspection of the spectrum, however, indicates that the signal does not contain relevant information beyond 6 GHz (results not shown). Compared with Heimovaara et al. (1996) who presented an input signal with a bandwidth of 3.5 GHz our signal has a much wider frequency range. One reason for this is that it appears that the TEKTRONIX 1502C emits a signal with a broader bandwidth at higher resolutions (our input waveform was determined for a cable-tester resolution of 0.1 m div^{-1} vs. 0.5 m div^{-1} in Heimovaara, 1994 and Heimovaara et al., 1996). Further, we determined our input function directly at the port of the cable tester. We therefore had no cable losses, which are proportional to $\sqrt{f}$ and are especially strong at higher frequencies (Davidson, 1978).

Scatter functions for the multi-layer systems were computed with Eq. [5] through [12] using the relevant segmentation information listed above. We set the zero-frequency permittivity (ε_s) of water at 25°C to 78.5 ε_o (where ε_o is the permittivity of vacuum); the permittivity of water at infinite frequency (ε_∞) was set at 4.22ε_o, and the relaxation frequency f_{rel} was set at 17 GHz. For the permittivity of the Acrylic we assumed a value of 2.76ε_o (Lide, 1993) for all frequencies.

Computed waveforms were calculated by Inverse Fourier Transforms of $R(f)$ (Eq. [4]), followed by a cumulative sum to counteract the back-difference operation used for the computation of V_0. Reflection times were calculated by computing waveforms with open-ended and shorted-end reflections. The time where the open and shorted waveforms diverged by more than 0.01 was taken as the end reflection. The beginning of the sensor was defined at the time where the waveforms diverged by 0.01 from the input waveform, $W(t)$ (Eq. [13]). Reflection times of single segment waveforms computed in this way diverged <0.01 ns from reflection times computed directly from sensor length and permittivity (results not shown).

We would like to stress that, contrary to the measurements, we did not "attach" a cable to our modeled probe, nor did we include a probe head (cable to probe transition). We also did not include effects of a cut-off frequency for transversal wave propagation through a probe (Ramo et al., 1984). The modeled system is therefore a highly idealized version of the probe used for the multi-layer probe and we did not try to fit computed and measured waveforms beyond using known probe length and geometry.

RESULTS AND DISCUSSION

Averaging with a TDR Probe in Air and Water

The first experiments were conducted to characterize the response of the TDR probe to different dielectric orientations. Figure 2 demonstrates the relative permittivity and EC measured using the TDR for probes with water and air. The three-rod probe was placed horizontal to the water–air interface with the central conductor half immersed in air and half in water. In theory both EC and permittivity should give the arithmetic average result for parallel connection. Measurements were made with the probe lying with all three electrodes on the interface between the water and air and with one electrode totally submerged and the other totally in air. The results demonstrate that this gives the arithmetic average permittivity or EC. The shape of the graph indicates a rapid transition to the permittivity of the material that the bulk of the probe is in as its orientation angle is changed. It is important to note that both the permittivity and EC are weighted in the same way for the parallel measurements; this is not the case for perpendicular measurements of EC and permittivity.

A follow up experiment was conducted with a probe inserted, perpendicular to a water bath. Figure 4 presents the results for a 20-cm probe inserted 1 cm at a time into the water. Both arithmetic average permittivity and refractive index average permittivity are plotted and the data clearly corresponds with the refractive index averaging regime.

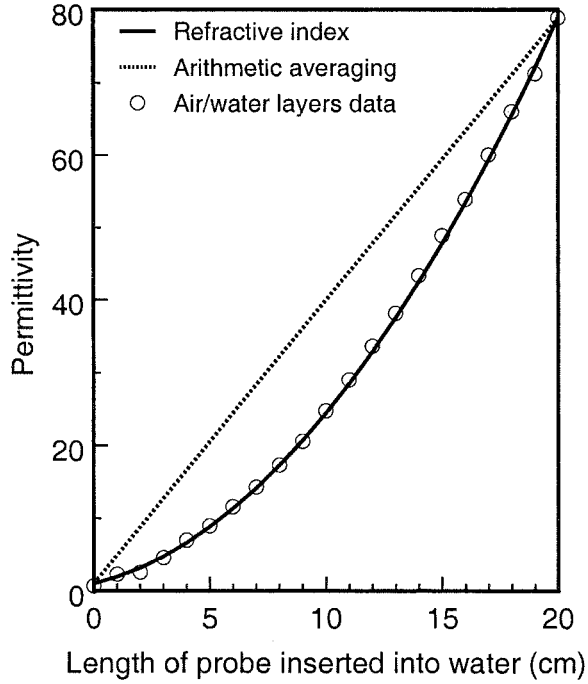

Fig. 4. Permittivity measured for two layers using a 20-cm probe sequentially inserted into water with the upper portion in air.

Averaging in a Three-Layered Homogeneous Material

The results for the three layers of white paraffin, water, and air are presented in Fig. 5. The configuration of three homogeneous layers arranged along the length of a TDR probe lends itself to theoretical analysis (Whalley, 1993). It takes the approach followed by Topp et al. (1982) and expands it for three layers. The expected results are plotted using the refractive index method according to the fractional lengths of the layers. The data suggest that again in this case of three layers the refractive index averaging regime is appropriate.

Multi-Layer TDR Signal Response

Results of the modeled waveforms are presented in Fig. 6 for a probe length of 30.24 cm. Figure 6A gives waveforms modeled assuming homogeneous media. The arithmetic (39.9) and refractive index (27.3) average permittivity values were calculated for a volume fraction of 0.5 water ($\varepsilon = 78.3$) and 0.5 Acrylic ($\varepsilon = 2.76$). Waveforms were calculated assuming a homogeneous material with the respective permittivity values; relaxation was assumed to occur at the same frequency as that of water (17 GHz). In Fig. 6B waveforms are presented for the same probe but now with thin multiple layers. Two layers represents one layer of Acrylic and one layer of water, 80 layers, 40 layers of each. A short was placed at the end of each probe in the computation to determine the exact end point for the reflection as the waveforms become more complex when more layers are present. Arrows are placed on the graph from the homogeneous media representing the refractive and arithmetic bounds. They indicate that for two layers the travel time is that for refractive index averaging where as

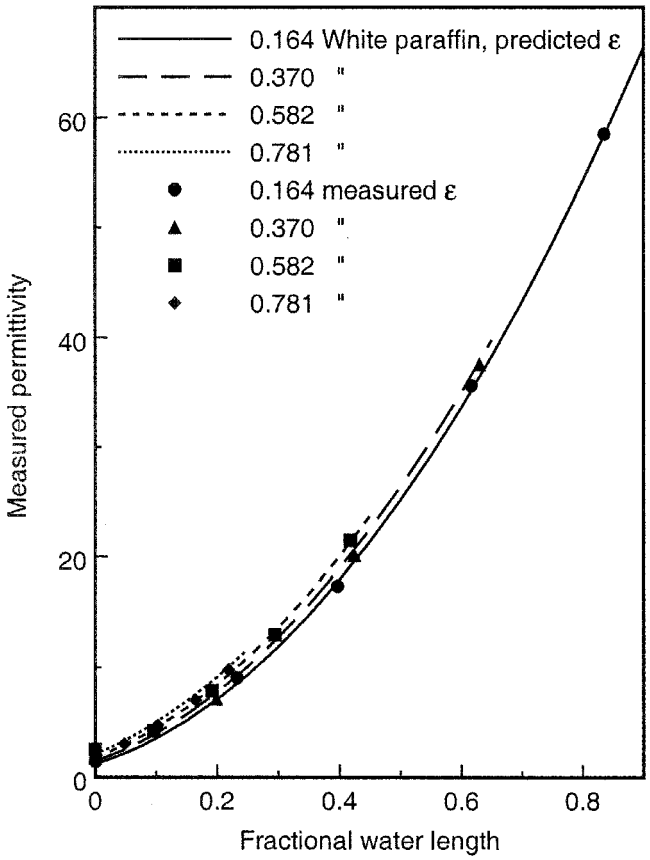

Fig. 5. Measurements of three layers, white paraffin, water, and air. The length fraction amounts of white paraffin are indicated and the lines are the predicted permittivity (ε) according to Eq. [2].

for multiple layers the travel time agrees with arithmetic averaging of the permittivity.

Figure 6C presents waveforms measured using Acrylic discs and water, the results show excellent qualitative agreement with Fig. 6B. There are small differences, which can be accounted for by the fact that no sensor head was used in the modeled results but was present for the measurements. The waveforms for the measurements are also a little more rounded suggesting a lower frequency content than the waveforms that were modeled. However, the overall qualitative agreement is very good. Results for these waveforms are presented in Fig. 7 and demonstrate that as the layer thickness decreases the apparent permittivity moves to the arithmetic average.

Figure 8 presents the measured travel times versus layer thickness for the measured data in terms of normalized velocity:

$$v_{\text{normalized}} = \frac{v_{\text{EMT}} - v_{\text{measured}}}{v_{\text{EMT}} - v_{\text{ray}}} \quad [14]$$

The upper bound of 1 corresponding to refractive index averaging (ray theory) and the lower bound of 0 corresponding to arithmetic averaging (EMT). Figure 8 also shows results by Chan and Knight (2001) who used wavelength over layer thickness. We chose not to use wavelength, as wavelength for a broadband signal is not well defined. We also show modeling results for the

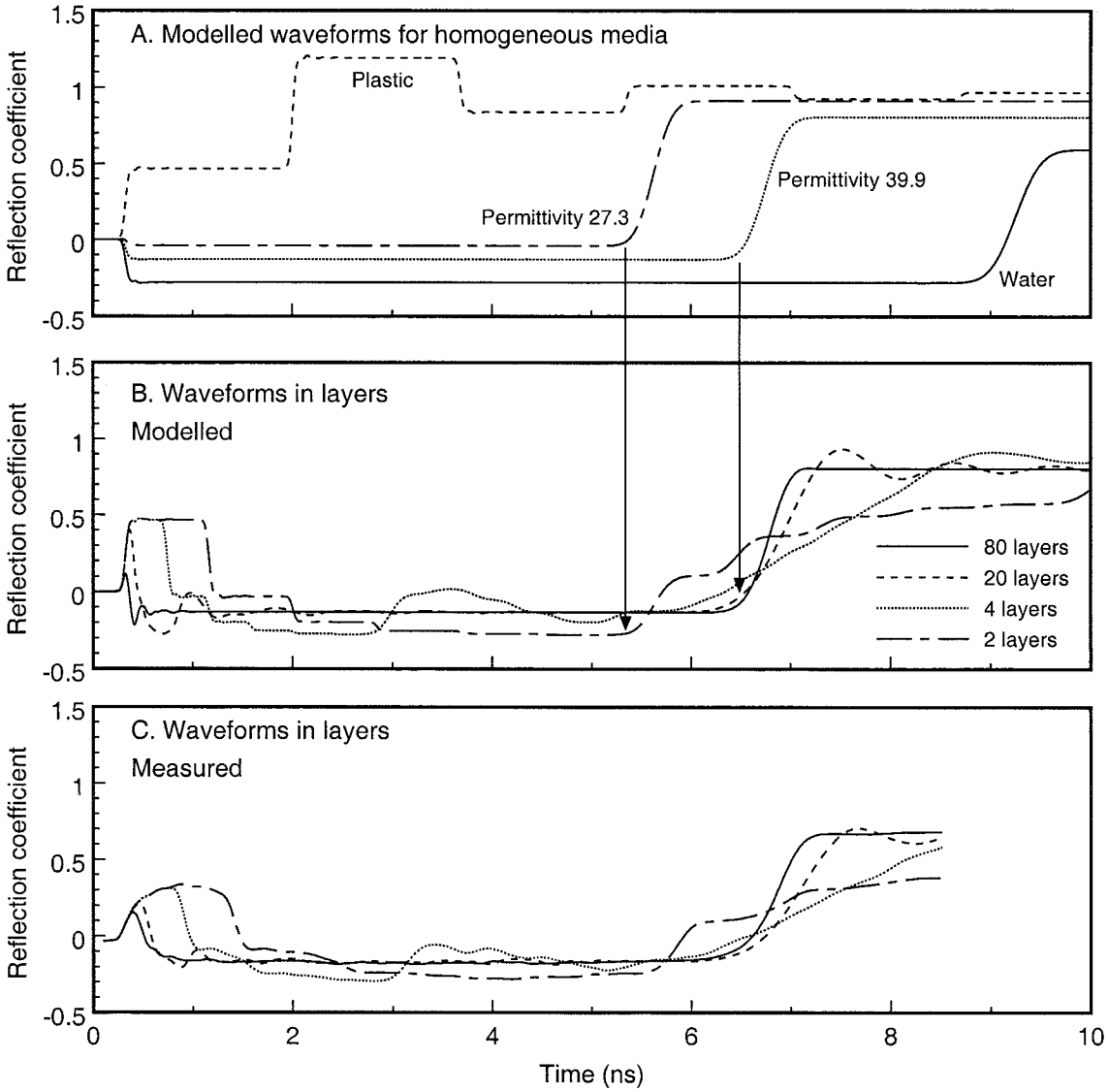

Fig. 6. Modelled and measured waveforms, (A) Modelled waveforms for homogeneous media, (B) Modelled waveforms for layered media, (C) Measured waveforms for layered media corresponding to those modelled in 6B.

idealized probe for 2, 4, … 98, and 100 layers. Although the model results and measurements do not match very well, all data indicate a transition from the refractive index averaging regime to the arithmetic when layers become thinner. The difference between our results, those of Chan and Knight (2001) and the model are considered to be due to differing frequency contents in the input signals, probe design, and experimental setup.

Although the measured and computed waveforms in Fig. 6 show good qualitative agreement they do not provide information as to why a transition from refractive to arithmetic averaging occurs for multi-layered systems. Chan and Knight (2001) suggested that a characteristic wavelength/layer thickness ratio affected the averaging transition, with a transition value of about 4. However, because TDR is a broadband method that includes frequencies up to a few GHz (Heimovaara, 1994, and this study), it is difficult to explain the averaging transition in terms of one wavelength. We believe that the explanation for the transition should be sought in the fact that the signal does not solely propagate straight to the end of the probe and back again to the beginning. Instead, many (partial) reflections occur at the impedance mismatches at segment boundaries. The multiple reflections cause the average signal path to lengthen causing an increase in the travel time. Subsequently, a longer travel time is interpreted as a higher *apparent* permittivity—even though the water content does not change. The question now becomes whether this delay occurs for all frequencies or whether certain frequencies are favored because of constructive or destructive interference. To this end we further analyzed the modeled results.

The scatter function for a transmission line contains all relevant information for signal losses and signal delay. The scatter function computed in Eq. [5] presents this information in terms of real and imaginary numbers that have a computational interpretation but not directly a meaning in a physical sense. However, by converting the scatter function to a polar form (i.e., by computing

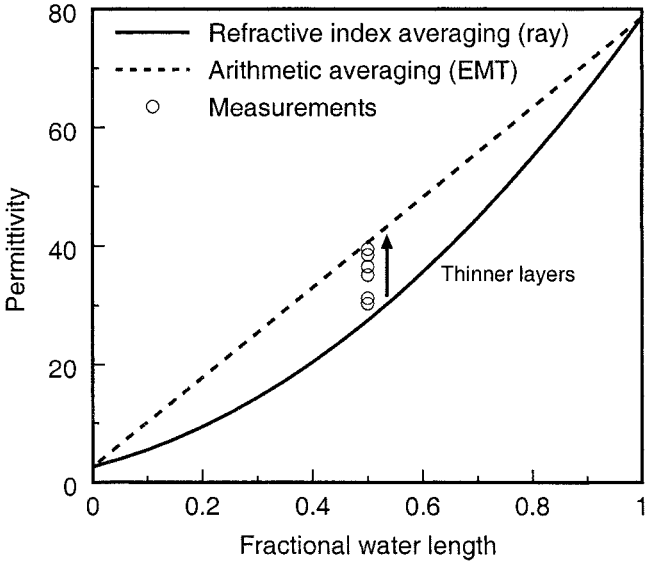

Fig. 7. Apparent permittivity increasing as the layers become proportionally thinner, refractive index and arithmetic averaging acting as bounds.

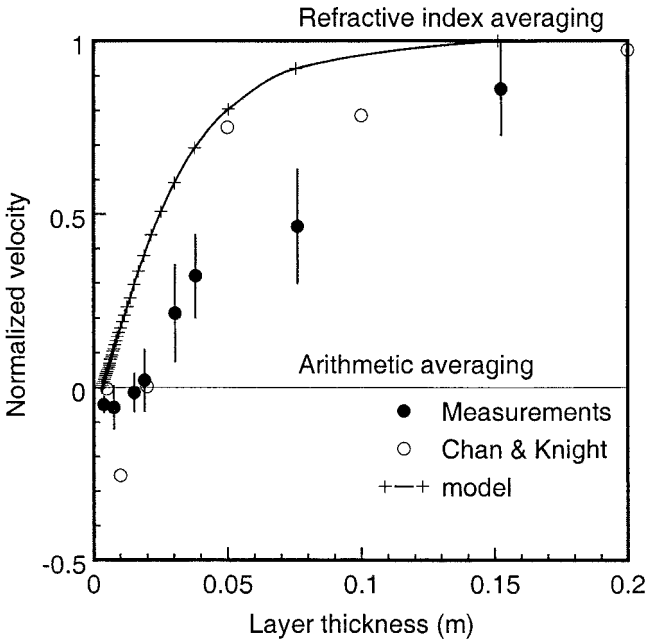

Fig. 8. Normalized wave velocity (Eq. [14]) as a function of layer thickness with bounds provided by the refractive index and arithmetic-averaging regime. Modeled results reflect 2,4,6…98,100 layers, with layers becoming proportionally thinner. Measurements of Chan and Knight (2001) for interchanging layers of wet and dry sand included.

a magnitude and a phase) more useful quantities can be derived. The magnitude (i.e., $|S_{11}|$) of the scatter function provides information about the relative dielectric losses, but is not useful for the following discussion. Phase information contains information on how much a transmission line delays a signal and can be computed by taking the complex argument of the $S_{11}(f)$ scatter function {i.e., arctan[im(S_{11})/re(S_{11})]}. The phase difference of a sinusoidal signal entering and leaving a transmission line of length L is $(2\pi fL\sqrt{\varepsilon_r})/c$ radians, where one complete cycle of the signal is 2π radians (or 360 degrees), ε_r is the relative permittivity and c the speed of light. For a perfectly matched cable-transmission line system with an open-ended reflection the phase difference is $(4\pi fL\sqrt{\varepsilon_r})/c$ as the distance L is traveled twice. The delay of the signal (in seconds) is simply calculated by dividing the phase difference by $2\pi f$.

In Fig. 9 we plotted the delay (left axis) and square root of the apparent permittivity (right axis) versus frequency for a 30.24-cm probe with 2, 4, 16, 40, and 80 layers. Also shown are two horizontal lines that represent the calculated delay for refractive and arithmetic averaging (ε_r equals 27.62 and 40.53, respectively). To produce the data for this figure we used the same probe and segmentation properties as used for Fig. 6B. However, to substantially simplify an otherwise very complicated graph we assumed that relaxation of water did not occur (i.e., the modeled system has no dielectric losses). Omission of free water relaxation does not substantially affect the following discussion.

The results in Fig. 9 are surprisingly complex. It appears that two- and four-layer systems roughly mimic refractive averaging for frequencies upward from about 500 MHz. For lower frequencies the departure from refractive averaging is larger, with the regime extending beyond arithmetic averaging, or even showing subrefractive behavior. At very low frequencies (<50 MHz) very high delays are shown. These partly result from impedance mismatches between the 50-ohm cable and the probe. High delays at low frequencies also occur for mismatched single layer systems (i.e., homogeneous systems) with an impedance below 50 ohms (results not shown). The high delays at low frequencies probably result from strong (negative) reflections off the beginning of the probe (see Eq. [6]). Conversely, we expect shorter delays when probe impedances are higher than 50 ohms. For the systems containing 16, 40, and 80 layers it appears that the averaging becomes more arithmetic by extending to higher and higher frequencies. However, for these also, the averaging is not purely arithmetic. Super arithmetic averaging may occur in certain frequency ranges, whereas for other frequencies the averaging may suddenly crossover to be more refractive-like, or even be subrefractive (e.g., the 16 layer system). The 40- and 80-layer systems show a similar pattern as the 16-layer system, but extended to higher frequencies.

When broadband methods are used it can be expected that refractive averaging will be found for two or four layer systems because the average delay over a frequency range is similar to that of the refractive regime. However, narrow-band or single frequency dielectric methods for these systems are unlikely to exhibit refractive averaging. Regimes below and above refractive averaging are then possible. Subrefractive averaging can be explained by reflection of most of the signal out of the probe before it reaches the end of the sensor (permittivities would appear to be too low). Super-refractive averaging indicates that the multiple reflections tend to "lock-up" the signal at certain resonance frequencies (permittivities appear to be too high). We note that for low frequencies, the two and four layer systems exhibit

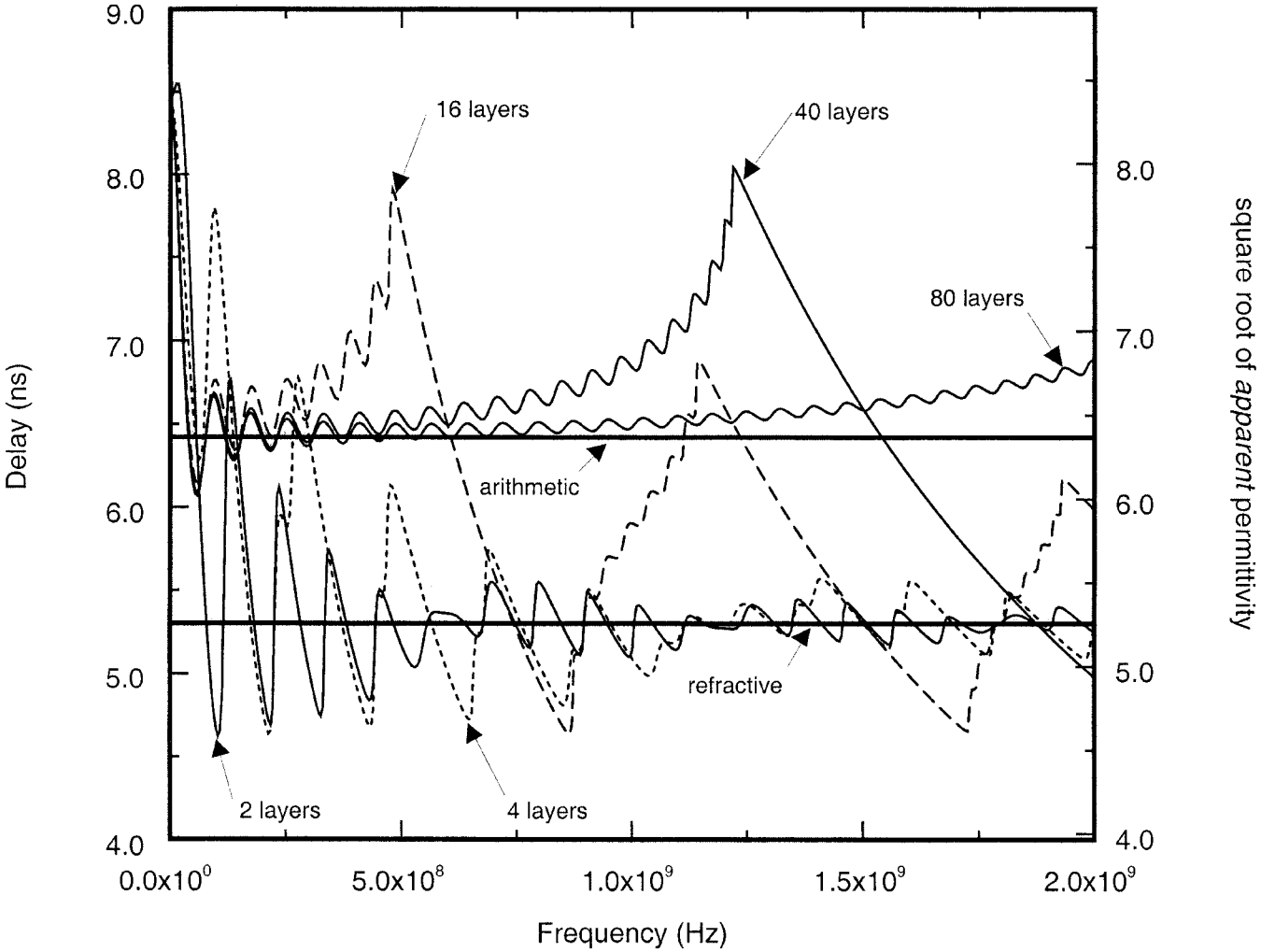

Fig. 9. Signal delay (left axis) and the root of the apparent permittivity (right axis) versus frequency. The horizontal lines represent the expected delay for refractive (lower line) and arithmetic averaging (upper line) for a volume with 50% Acrylic and 50% water. Because the probe length was 30.24 cm the numerical values in left and right axes are nearly identical.

more arithmetic-like averaging regimes, qualitatively confirming Chan and Knight (2001). Depending on the bandwidth of the method used it seems that multi-layer systems are more likely to exhibit arithmetic averaging, only at very high frequencies these systems will show refractive averaging. The arithmetic regime can be explained by the increased likelihood that multi-layer systems will exhibit signal resonance at the many impedance mismatches that exist within the probe, which tends to increase the delay and hence to increase the apparent permittivity.

We would like to note that the scenario presented in Fig. 6 through 9 represents a rather extreme case of permittivity contrasts (ε_r equals 2.76 for Acrylic and around 80 for water). Real world applications in soils or sediments will most likely have much smaller contrasts such as a permittivity of 3 to 5 for completely dry soil to 25 or 35 for completely saturated media, but be smaller still in most cases. Nevertheless, the complex transition from refractive to arithmetic will most likely occur for such systems as well and will roughly scale with the root of the permittivities involved. Finally, we would like to note that the transition from refractive to arithmetic averaging is affected by many factors, such as sensor length and geometry (including impedance), permittivity of the porous material, thickness and periodicity in layering (or lack thereof), and the bandwidth of the dielectric method used. The results presented in Fig. 9 are but for one probe design and results are likely to be qualitatively and quantitatively different in other circumstances.

CONCLUSIONS

Measurement and modeling results of this study indicate that refractive averaging of dielectric properties over the length of a TDR probe cannot always be relied on. Our measurements show that arithmetic averaging results when dielectric materials are layered in parallel with the probe. Refractive averaging is mostly prevalent when a small number of thick layers are oriented perpendicular to the probe. In contrast, multi-layer systems commonly exhibit arithmetic averaging, which we attribute to signal delay because of resonance within the

multi-layers. We showed that measured and modeled TDR waveforms for multi-layer probes showed good agreement. A further evaluation of the scatter functions that were computed for the waveform modeling shows that the averaging regime exhibits a complex frequency-dependent pattern. We also show that broadband dielectric methods are more likely to exhibit "pure" refractive or arithmetic averaging. Narrow-band methods may be particularly sensitive to layering within the probe length and may produce erroneous results if refractive averaging is relied on.

ACKNOWLEDGMENTS

This research was supported in part by research grant No. IS-2839-97, from BARD. The United States–Israel Binational Agricultural Research and Development Fund, and in part by a grant from the USDA NRi grant program (2002-35107-12507). M.G. Schaap was supported, in part, by the SAHRA science and technology center under a grant from NSF (EAR-9876800).

REFERENCES

Birchack, J.R., C.Z.G. Gardner, J.E. Hipp, and J.M. Victor. 1974. High dielectric constant microwave probes for sensing soil moisture. Proc. IEEE 62:93–98.

Björck, S., I. Cato, L. Brunnberg, and B. Strömberg. 1992. The clay-varve based Swedish time scale and its relation to the Late Weichselian radiocarbon chronology. p. 25–44. *In* E. Bard and W.S. Broecker (ed.), The last deglaciation: Absolute and radiocarbon chronologies. NATO ASI Series. I, Vol. 2, Springer-Verlag, Berlin.

Chan, C.Y., and R. Knight. 1999. Determining water content and saturation from dielectric measurements in layered materials. Water Resour. Res. 35:85–93.

Chan C.Y. and R. Knight, 2001. Laboratory measurements of electromagnetic wave velocity in layered sands. Water Resour. Res. 37, 4:1099–1105.

Dasberg, S., and J.W. Hopmans. 1992. Time domain reflectometry calibration for uniformly and non-uniformly wetted sandy and clayey loam soils. Soil Sci. Soc. Am. J. 56:1341–1345.

Davidson, C.W. 1978. Transmission lines for communications. John Wiley & Sons, New York.

Feng, W., C.P. Lin, R.J. Deschamps, and V.P. Drnevich. 1999. Theoretical model of a multiscetion time domain reflectometry measurement system. Water Resour. Res. 35:2321–2331.

Hayhoe H.N., W.G. Bailey and G.C. Topp, 1983. Measurement of soil water contents and frozen soil depth during a thaw using time-domain reflectometry. Atmos. Ocean. 21:299–311.

Heimovaara, T.J. 1993. Design of triple-wire time domain reflectometry probes in practice and theory. Soil Sci. Soc. Am. J. 57:1410–1417.

Heimovaara, T.J., and E. de Water. 1993. A computer controlled TDR system for measuring water content and bulk electrical conductivity of soils. Rep. 41 Laboratory of Physical Geography and Soil Science, University of Amsterdam, Nieuwe Prinsengracht 130 1018 VZ Amsterdam.

Heimovaara, T.J. 1994. Frequency domain analysis of time domain reflectometry waveforms: 1. Measurement of complex dielectric permittivity of soils. Water Resour. Res. 30:189–199.

Heimovaara, T.J., E.J.G. de Winter, W.K.P. van Loon, and D.C. van Esveld. 1996. Frequency-dependent permittivity from 0 to 1 GHz: Time domain reflectometry measurements compared with frequency domain network analyzer measurements. Water Resour. Res. 32:3603–3610.

Huisman, J.A., C. Sperl, W. Bouten, and J.M. Verstraten. 2001. Soil water content measurements at different scales: Accuracy of time domain reflectometry and ground-penetrating radar. J. Hydrol. (Amsterdam) 245:48–58.

Huisman, J.A., A.H. Weerts, T.J. Heimovaara, and W. Bouten, 2002. Comparison of travel time analysis and inverse modeling for soil water content determinations with time domain reflectometry. Water Resour. Res. 38, 10.1029/2001WR000259.

Lide, D.R., 1993. Handbook of chemistry and physics, 74th ed. 1993–1994. CRC Press Inc., Boca Raton, FL.

Nadler, A., S. Dasberg, and I. Lapid, 1991. Time domain reflectometry measurements of water content and electrical conductivity of layered soil columns. Soil Sci. Soc. Am. J. 55:938–943.

Ramo, S., R. Whinnery, and T. Van Duzer. 1984. Fields and waves in communication electronics. Wiley, New York.

Robinson, D.A., M. Schaap, S.B. Jones, S.P. Friedman, and C.M.K Gardner. 2003. Considerations for improving the accuracy of permittivity measurement using TDR: Air-water calibration, effects of cable length. Soil Sci. Soc. Am. J. 67:62–70.

Stein J. and D.L. Kane, 1983. Monitoring the unfrozen water content of soil and snow using time domain reflectometry. Water Resour. Res. 19: 1573–1584.

Todoroff, P., and J.D. Lan Sun Luk. 2001. Calculation of in situ soil water content profiles from TDR signal traces. Meas. Sci. Technol. 12:27–36.

Topp, G.C., J.L. Davis, and A.P. Annan. 1980. Electromagnetic determination of soil water content: measurements in coaxial transmission lines. Water Resour. Res. 16:574–582.

Topp, G.C., J.L. Davis, and A.P. Annan. 1982. Electromagnetic determination of soil water content using TDR: I. Applications to wetting fronts and steep gradients. Soil Sci. Soc. Am. J. 46:672–678.

Whalley W.R., 1993. Considerations on the use of time domain reflectometry (TDR) for measuring soil water content. J. Soil Sci. 44: 1–9.